Accepted Manuscript

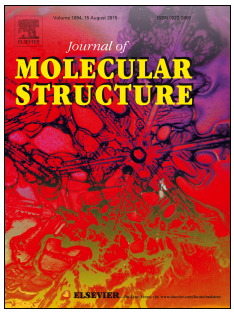

Long-range anisotropic effects in a V–shaped Tröger's base diformanilide: Conformational study by NMR assignment and DFT calculations

Leandro Trupp, Sergio L. Laurella, M. Cristina Tettamanzi, Beatriz C. Barja, Andrea C. Bruttomesso

PII: S0022-2860(17)31580-6

DOI: 10.1016/j.molstruc.2017.11.092

Reference: MOLSTR 24579

To appear in: *Journal of Molecular Structure*

Received Date: 23 August 2017

Revised Date: 21 November 2017

Accepted Date: 21 November 2017

Please cite this article as: L. Trupp, S.L. Laurella, M.C. Tettamanzi, B.C. Barja, A.C. Bruttomesso, Long-range anisotropic effects in a V–shaped Tröger's base diformanilide: Conformational study by NMR assignment and DFT calculations, *Journal of Molecular Structure* (2018), doi: 10.1016/j.molstruc.2017.11.092.

Graphical Abstract

To create your abstract, type over the instructions in the template box below.
Fonts or abstract dimensions should not be changed or altered.

Long-range anisotropic effects in a V–shaped Tröger's base diformanilide: conformational study by NMR assignment and DFT calculations

Leave this area blank for abstract info.

Leandro Trupp, Sergio L. Laurella, M. Cristina Tettamanzi, Beatriz C. Barja and Andrea C. Bruttomesso

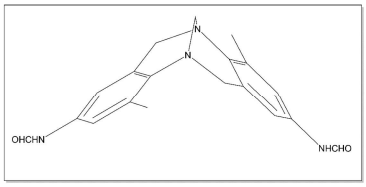

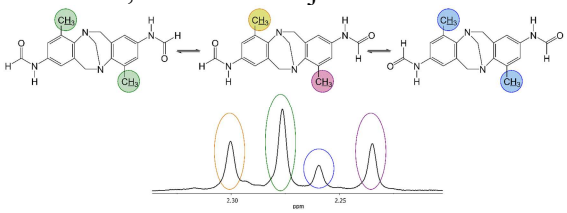

ELSEVIER

Journal of Molecular Structure
journal homepage: www.elsevier.com

Long-range anisotropic effects in a V–shaped Tröger's base diformanilide: conformational study by NMR assignment and DFT calculations

Leandro Trupp[a,d], Sergio L. Laurella[b], M. Cristina Tettamanzi[c,1], Beatriz C. Barja[d] and Andrea C. Bruttomesso[a,*]

[a]*DQO – UMYMFOR, FCEN, UBA, Int. Güiraldes 2160, Ciudad Universitaria, Buenos Aires, 1428, Argentina*
[b]*CEQUINOR, DQ, FCE, UNLP, 47 y 115 s/n, La Plata, 1900, Argentina*
[c]*Dept. of Chemistry and Biochemistry, USciences, 600 S. 43rd St., Philadelphia, PA 19104, USA*
[d]*DQIAQF – INQUIMAE, FCEN, UBA, Int. Güiraldes 2160, Ciudad Universitaria, Buenos Aires, 1428, Argentina*

ARTICLE INFO

Article history:
Received
Received in revised form
Accepted
Available online

Keywords:
Tröger´s base
Diformanilide
Conformational analysis
Long-range anisotropy
NMR spectroscopy
Theoretical calculations
Variable Temperature NMR
Line shape analysis

ABSTRACT

Herein we describe the synthesis and conformational analysis of a Tröger's base diformanilide whose distinctive NMR spectra was fully assigned via DFT calculations. The complexity of the spectra originated by the presence of three conformers in equilibrium shows that the nuclei in each side of the molecule are sensitive to the configuration not only of the closest formamide moiety but also of the farthest one, due to long–range anisotropic effects. The temperature and the solvent polarity influence were analyzed to determine the different conformer populations and the corresponding rotational activation parameters.

[1] Present address: Dept. of Chemistry, College of Science and Technology, Temple University, 1901 N. 13th St., Philadelphia, PA 19122, USA

* Corresponding author. Tel.: +54-11-4576-3346; fax: +54-11-4576-3346; e-mail: aachiocc@qo.fcen.uba.ar

1. Introduction

Building blocks with well-defined rigid structures are very convenient in organic synthesis, as they allow the control and disposition of different substituents in predictable geometries. 6*H*,12*H*–5,11–methanodibenzo[*b*,*f*][1,5] diazocine –Tröger's base (TB)– is one of the most used compounds of this kind, because it adopts a rigid V–shaped geometry with the aromatic rings almost perpendicular to each other (Figure 1) [1–3]. These molecules present both practical and theoretical interest, their applications being particularly useful in areas such as molecular recognition, drug development, bioorganic and supramolecular chemistry and for optical and optoelectronic device design [4–11].

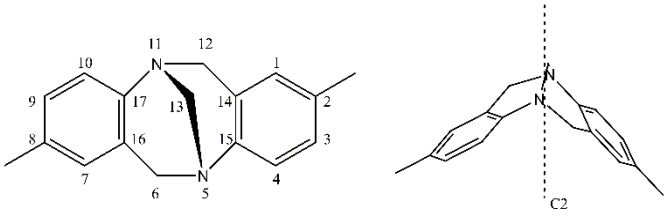

Figure 1. Molecular structure of (*S,S*)-Tröger's base and numbering according to its systematic name.

Although TB was first synthesized in 1887 by Carl Julius Tröger, in the last few decades there has been an important resurgence in the study of the synthesis and characterization of different TB derivatives due to their unique properties, which even led them to be described as one of the "fascinating molecules in organic chemistry" [12].

TB consists of two aromatic rings fused by a bicyclic aliphatic methanodiazocine unit whose methylene bridge prevents pyramidal inversion of the two nitrogen atoms and thus makes them stable stereogenic centers. The aromatic rings stand in a nearly perpendicular fashion with an angle which has been predicted for a wide array of derivatives between 84° and 105°, with a mean value of 95.3°, and a minimum distance of approx. 1 nm between the substituents [13,14]. This fixed configuration makes TB a C2-symmetric chiral molecule with a hydrophobic cavity, which can exist as the *RR* and *SS* enantiomers. The diastereomeric-TB (*RS*) is geometrically not viable.

Communication through space between the aromatic moieties in the V–shaped structure and its substituents has been studied in regard to the atropoisomerism in torsion balances [15–17]. In addition, in a TB bistriarylamine derivative our group found that, besides the geometrical connecting role, this non-conjugated bridge can surprisingly play an important electronic connecting role. Electrochemical and EPR measurements as well as CAM-B3LYP calculations performed showed an unexpectedly large capacity of the aliphatic bridge to electronically connect the arylamines, reflected in the spin and charge distribution. The main factor that originates this electronic connection is the rigid geometry of the bridge that makes the nitrogen atoms face each other, and therefore the lone pairs enter the bridge and overlap with the arylamine π-system [18,19]. Regarding the possible communication of the aromatic rings through space, to the best of our knowledge no experimental study has been reported of TB's diamide bond conformers.

The amide group may act as a probe to detect long range interactions. In fact, if different conformations arising from these two distant amide moieties can be discriminated by NMR, the analysis of these signals can give valuable information regarding the possibility of long-range anisotropic effects in the system. The large rotational energy barrier around the N–C(O) bond caused by its partial double bond character generates non-equivalent substituents. This rotation is usually slow on the ^{1}H NMR time scale at room temperature, enabling the *Z* (*cis*) and *E* (*trans*) conformers to be distinguished [20].

The assignment of the 1D NMR signals to each conformer may be done from identification of the CHO proton peaks, which are recognized from the CHO–NH couplings of approximately 11.0 Hz (*cis* isomer) and 1.5 Hz (*trans* isomer) [20]. The TB skeleton presents, in principle, a characteristic and relatively simple ^{1}H NMR, corresponding to the aromatic and bridge protons. The bridgehead methylene (C13) appears as a singlet between the non-equivalent non-bridgehead methylene signals, of which the *endo* protons appear more shielded than the *exo* ones [13].

In this work, we describe the synthesis and complete analysis of the 1D and 2D NMR spectra of a model diformamide TB derivative **1** (*N,N'*-((5S,11S)-4,10-dimethyl-6H,12H-5,11-methanodibenzo[b,f][1,5] diazocine-2,8-diyl) diformamide), whose complex array of signals is consistent with the presence of long-range anisotropic effects that confirm that both sides of the TB base skeleton are not independent from each other.

2. Results and discussion

2.1. Chemistry

Compound **3** was prepared in two steps according to literature procedures [21], starting from an acid–catalyzed condensation step of 2-methyl-4-nitroaniline with $(CH_2O)_n$ to obtain 2,8-dinitro Tröger's base derivative **2**, which is further reduced to the diamino substituted compound **3**. This compound was *N,N'*-diformylated to finally obtain the 2,8-diformamido TB derivative **1** (Scheme 1) [22]. **1** was characterized by mass spectrometry (HR-ESI) and 1D and 2D NMR spectroscopy. Spectra were obtained in different solvents and at several temperatures.

2.2. Conformational analysis and NMR assignment in chloroform

Observation of the amide bond configuration (*E* or *Z*) of both formamide units of **1** indicates the potential coexistence of three conformers in equilibrium, *EE*, *ZZ* and *EZ*, which can be differentiated by NMR spectroscopy if the N–C(O) bond rotation is slow enough. The fourth possible conformer (*ZE*) is the same as *EZ*, due to the C2 symmetry axis in the molecule (Figure 2), and all conformers are actually the racemic mixture of the *RR* and *SS* enantiomers, which cannot be discriminated by NMR. This analysis assumes free rotation around Ar–N bonds, as hindered rotation for these bonds is usually described only for 2-substituted tertiary anilides [23–25]. Each formamide is denoted as *E(E)*, *Z(Z)*, *E(Z)* and *Z(E)* according to its own configuration and to the other one, specified between brackets.

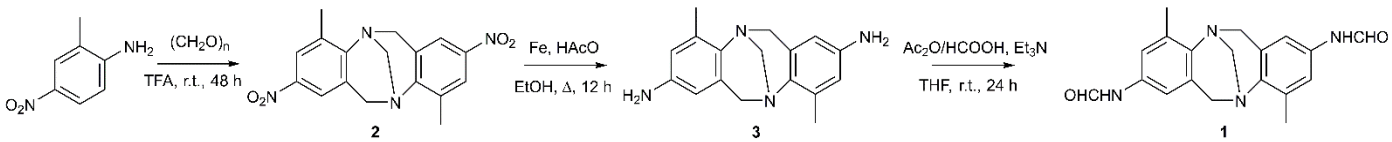

Scheme 1. Synthesis of N,N'–((5S,11S)–4,10–dimethyl–6H,12H–5,11–methanodibenzo[b,f][1,5]diazocine–2,8–diyl)diformamide **1** starting from 2–methyl–4–nitroaniline

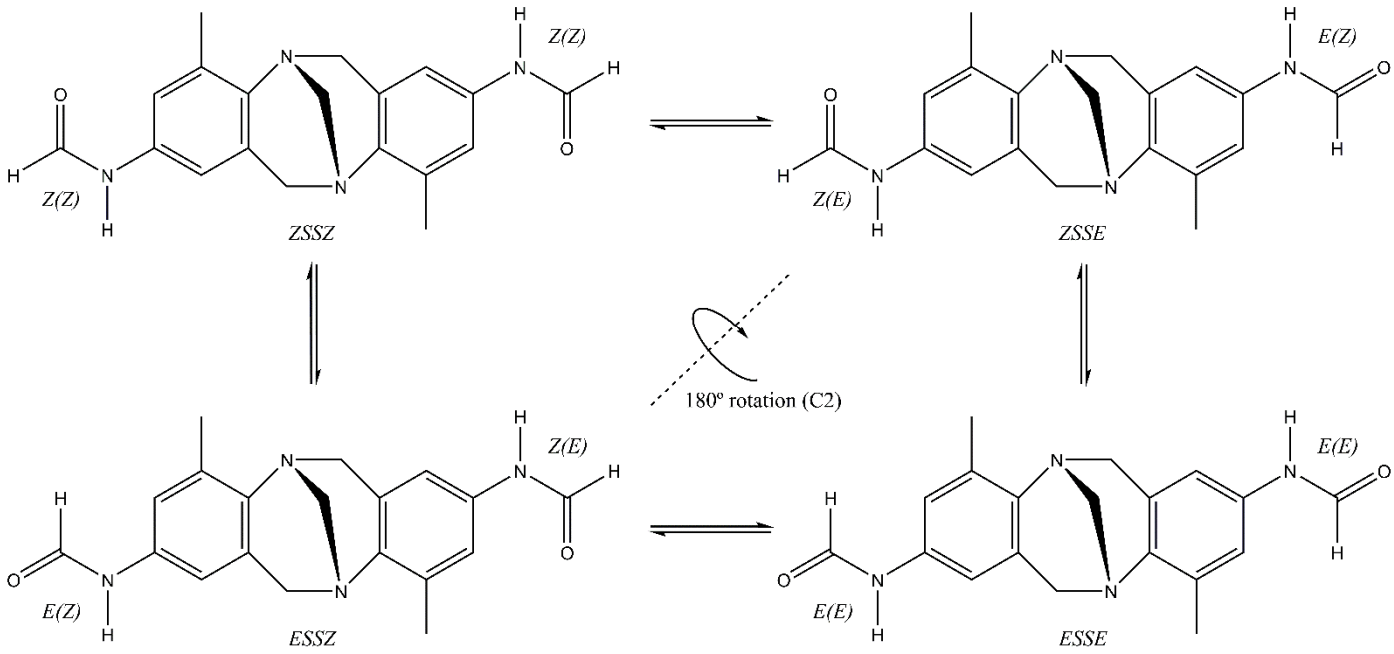

Figure 2. Amide bond conformers of **1**. Species *ZSSE* and *ESSZ* are the same, through a 180º rotation around the C2 symmetry axis. Each formamide is denoted according to its own configuration and to the other one, specified between brackets. (*S,S*) and (*R,R*) enantiomers are indistinguishable by NMR experiments and thus the latter are omitted here for clarity.

Figure 3 shows the experimental ^{1}H NMR spectrum of **1** in $CDCl_3$ at 25°C, where the number of peaks shows that the nuclei in each side of the molecule are sensitive to the configuration not only of the closest formamide but also of the farthest one, which is up to 12 bonds apart (see detailed analysis below). This long-range anisotropic effect originated by the formamide groups gives rise to four different proton peaks for each nucleus, one for each *EE* and *ZZ* conformer and two for the *EZ* one, given that both sides of the molecule are different. This effect is also visible in ^{13}C NMR (Figs. S1–S3), where the presence of four magnetically non–equivalent sets of nuclei are detected for most signals.

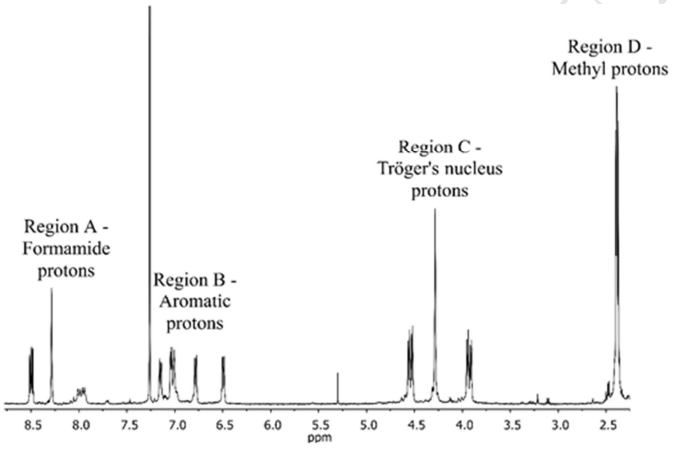

Figure 3. ^{1}H NMR spectrum of **1** in $CDCl_3$ at 25 °C.

Slow rotation around the N–C(O) bond and interconversion of conformers is confirmed by 2D EXSY spectra, as a cross peak with opposite phase to NOE correlations is observed for several protons from and close to *E* and *Z* formamides. These signals show magnetization transfer between two sites that undergo chemical exchange, and indicate that conversion between the different conformers is in fast exchange on the relaxation time scale, even when it is in the slow exchange limit on the NMR chemical shift time scale [26].

To the best of our knowledge, a complete conformer elucidation of this kind has not been done for any diformanilide. This conformational behavior is infrequent in oligoamides, as usually it is not possible to discriminate all the present conformers at room temperature, given that their populations are not similar, their NMR signals are identical or the N–C(O) bond rotation is not slow enough to be in the slow exchange regime [23,27–38]. Chen et al. [39] have synthesized a fluorene diformamide derivative whose 1D NMR spectrum in $CDCl_3$ apparently shows a similar behavior, but it has not been analyzed in detail.

In order to completely assign the experimental signals of each nuclei to the corresponding conformer, the species under study were subjected to geometry optimization using density functional theory (DFT) and calculations at the B3LYP/6–31G(d,p) level, taking into account dielectric solvent effects with the SCRF-PCM model. The isotropic chemical shifts for hydrogen and carbon atoms were obtained using the GIAO method [13,20,40–46].

The experimental spectra were subdivided in four regions A–D for a detailed discussion and assignment of the peaks, considering both bidimensional NMR spectra (Figs. S4–S11) and theoretical calculations. Experimental and calculated ^{13}C signals are shown in Table S1.

Region A – Formamide protons

Figure 4 shows the formamide region of the ^{1}H NMR spectrum of **1**. Only three signals are observed for each proton (two for the *E* formamides and one for the *Z* ones), as the signals of the *Z* formamides do not depend significantly on the other formamide configuration. The assignment of the NH protons is supported by COSY (Figs. S4–S5). EXSY spectrum confirms the exchange of the formamide protons (both CHO and NH) by the presence of a cross peak due to magnetization transfer (Fig. S10). In the ^{13}C NMR spectrum the four expected carbonyl signals are observed, more clearly separated for the *E* conformation (Fig. S2).

Table 1 summarizes the observed and calculated chemical shifts using DFT. The calculations not only permit the assignment of the signals with respect to the farthest formamide (higher or lower chemical shifts) but also give good predictions for almost all the signals, with deviations of less than 0.2 ppm

(except for the NH proton in the *E* formamides). It can also be predicted if two signals will give rise to two separate peaks or to only one, as in every case of the *E* formamide the calculated difference between peaks is larger than 0.01 ppm while for the *Z* formamide it is smaller than 0.01 ppm.

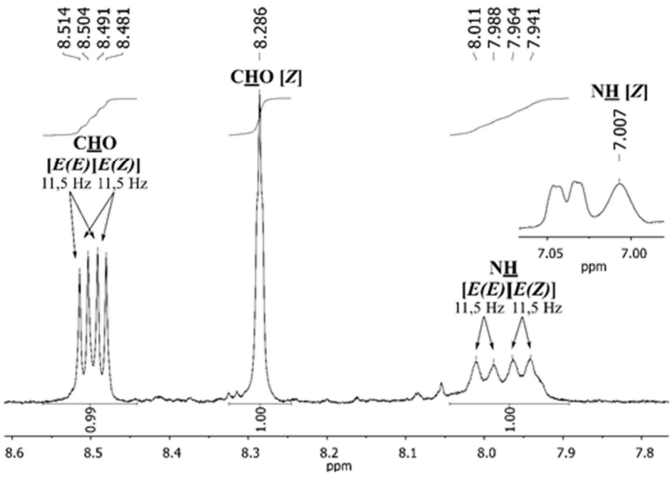

Figure 4. Formamide protons (Region A) of the ^{1}H NMR spectrum of **1** in $CDCl_3$ at 25 ˚C.

Table 1. ^{1}H NMR experimental and calculated chemical shifts for formamide protons of **1** in $CDCl_3$ at 25 °C, according to their own and farthest formamide configuration.

Own config.		*E*			*Z*		
Farthest config.		*E*	*Z*	diff.	*E*	*Z*	diff.
δ_{exp} / ppm	CHO	8.503	8.493	0.010	8.286		0.000
	NH	8.000	7.952	0.047	7.007		0.000
δ_{calc} / ppm	CHO	8.660	8.646	0.014	8.500	8.494	0.006
	NH	7.205	7.194	0.011	6.976	6.982	0.006

Region B – Aromatic protons

Figure 5 shows the aromatic region of the ^{1}H NMR spectrum, where eight different doublets with J_m = 1.5 Hz are observed (the singlet at 7.04 ppm corresponds to the NH proton of the *Z* formamide). Each signal can be assigned to a specific configuration of both formamides, based on the theoretical calculations and 2D spectra.

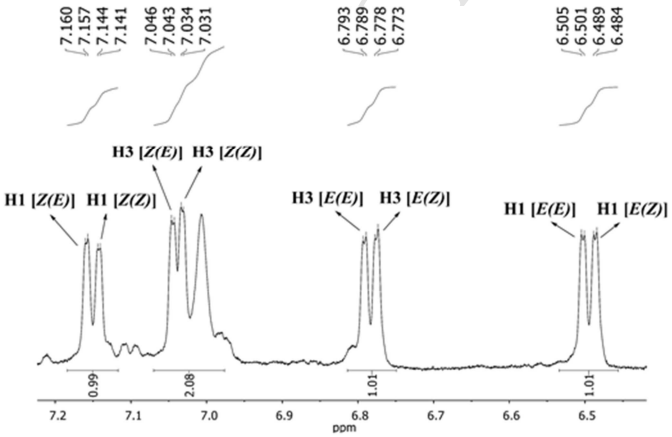

Figure 5. Aromatic protons (Region B) of the ^{1}H NMR spectrum of **1** in $CDCl_3$ at 25 ˚C.

Table 2 summarizes the experimental and calculated chemical shifts for each proton. In this case, there is some discrepancy between theoretical calculations and experimental chemical shifts of the aromatic protons that correspond to a *Z* formamide moiety; such difference could be overcome regarding vibrational effects (that were not taken into account when carrying out the calculations). The assignment relies on the NOE signals observed in the NOESY spectrum (Fig. S9), where the aromatic signals at ca. δ 6.50 and 7.20 ppm show a positive NOE effect with the *endo*–Tröger proton at 3.95 ppm; and the aromatic signals at ca. δ 6.80 and 7.05 ppm show a positive NOE effect with the methyl protons at 2.40 ppm. NOESY spectrum also confirms that Ar–N bond rotation is fast in the NMR timescale, as there is correlation between the NH (*E*) peaks and both aromatic protons (δ 6.50 and 6.78 ppm).

Table 2. ^{1}H NMR experimental and calculated chemical shifts for aromatic protons of **1** in $CDCl_3$ at 25 °C, according to closest and farthest formamide configuration.

Closest configuration		*E*		*Z*	
Farthest configuration		*E*	*Z*	*E*	*Z*
δ_{exp} / ppm	H1 / H7	6.503	6.487	7.159	7.413
	H3 / H9	6.791	6.776	7.045	7.033
δ_{calc} / ppm	H1 / H7	6.638	6.630	7.267	7.252
	H3 / H9	6.960	6.950	7.596	7.584

The four signals for each carbon can be seen in the ^{13}C NMR spectrum (Fig. S3). The shown assignments with respect to the closest formamide were done considering 2D correlations (HSQC or HMBC).

Region C – Tröger's nucleus protons

The Tröger's nucleus protons region of the ^{1}H NMR spectrum of **1** is shown in Figure 6, with the peaks assignment considering the predicted δ values shown in Table 3. The discrimination of *exo* and *endo* protons was also carried out considering the positive NOE effect between the methyl group and the *endo* protons and that between the bridgehead methylene H13 and the *exo* protons (Fig. S9). The fact that these hydrogens appear as two doublets (and not four) indicates that these methylene groups are affected by the configuration of the closest formamide but not by the farthest one, whereas the methylene bridge is not sensitive to any formamide configuration. This analysis is in agreement with the calculated values, with differences lower than 0.01 ppm for experimentally undistinguishable signals.

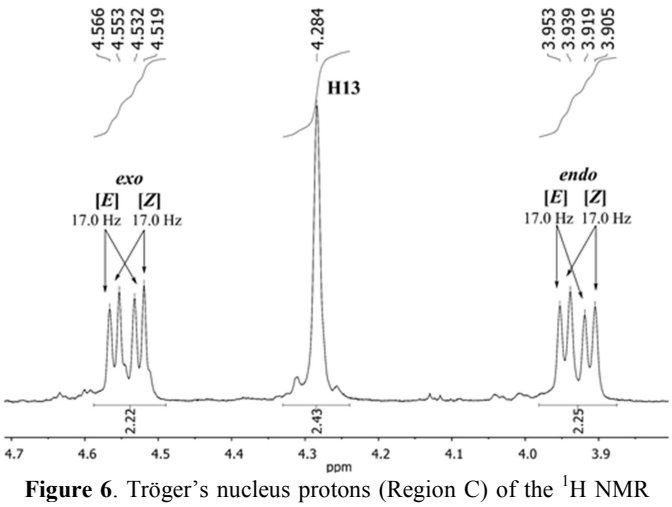

Figure 6. Tröger's nucleus protons (Region C) of the ^{1}H NMR spectrum of **1** in $CDCl_3$ at 25 ˚C.

Table 3. ^{1}H NMR experimental and calculated chemical shifts for Tröger's nucleus protons of **1** in $CDCl_3$ at 25 °C, according to closest and farthest formamide configuration.

Closest configuration		*E*		*Z*	
Farthest configuration		*E*	*Z*	*E*	*Z*
δ_{exp} / ppm	*endo*	3.936		3.922	
	exo	4.549		4.536	
	bridge	4.284			
δ_{calc} / ppm	*endo*	3.815	3.813	3.805	3.802
	exo	3.368	3.364	3.346	3.349
	bridge	4.001	3.997	3.992	3.985

Region D – Methyl protons

Figure 7 shows the methyl region of the ^{1}H NMR spectrum, where these protons can be seen affected by the configuration of both formamides and thus appear as four singlets. The experimental and calculated chemical shifts are shown in Table 4. Deconvolution of peaks using the MestReNova software is consistent with the assignment obtained from theoretical calculation, as the signals at 2.374 and 2.391 ppm have very similar integration and thus may belong to the same conformer.

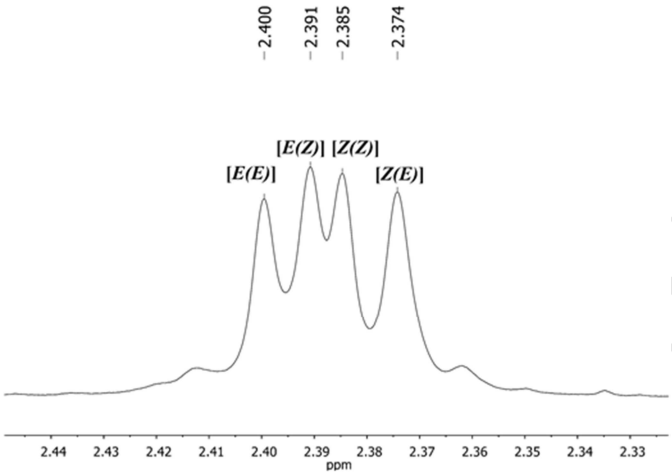

Figure 7. Methyl protons (Region D) of the ^{1}H NMR spectrum of **1** in $CDCl_3$ at 25 ˚C.

Table 4. ^{1}H NMR experimental and calculated chemical shifts for methyl protons of **1** in $CDCl_3$ at 25 °C, according to closest and farthest formamide configuration.

Closest configuration	*E*		*Z*	
Farthest configuration	*E*	*Z*	*E*	*Z*
δ_{exp} / ppm	2.400	2.391	2.374	2.385
δ_{calc} / ppm	2.304	2.298	2.269	2.282

2.3. Solvent effect in ^{1}H NMR spectra

The effect of solvent polarity on the spectrum of compound **1** was analyzed to study the extension of the anisotropic effects, as well as the different conformer populations. The ^{1}H NMR spectra in more polar solvents (DMSO–d_6, CD_3CN, CD_3OD, acetone–d_6 and DMF–d_7) are simplified and usually only one peak is observed for each proton close to an *E* or *Z* configuration, regardless of the farthest formamide's configuration. This result is in agreement with all spectra described in DMSO-d_6 for diformanilides connected by different spacers, such as –$S(O)_2$– [27], –C_2H_4– [28], –O– [29] or –S_2– [30] among others [31]. In $C_6D_6/CDCl_3$, on the other hand, the signals become even more complex than in $CDCl_3$.

Figure 8 shows the ^{1}H NMR spectra for the methyl region. For the least polar solvents ($C_6D_6/CDCl_3$ mixture, $CDCl_3$ and acetone–d_6) the spectra consist of the four peaks as expected for the *E(E)*, *Z(Z)*, *E(Z)* and *Z(E)* methyl protons. The relative order of chemical shifts varies with the solvent, and the assignment may be done on the basis of the integration knowing the overall *Z/E* ratio and that *E(Z)* and *Z(E)* peaks should have the same area. Nevertheless, in more polar solvents fewer peaks are observed: only two signals dominate the spectra in CD_3OD and CD_3CN –corresponding to the *Z* or *E* configuration of the closest formamide– while only one broad band with three shoulders is present in DMSO–d_6. Similar behavior is observed for the other regions of the spectra (Figs. S12–S13).

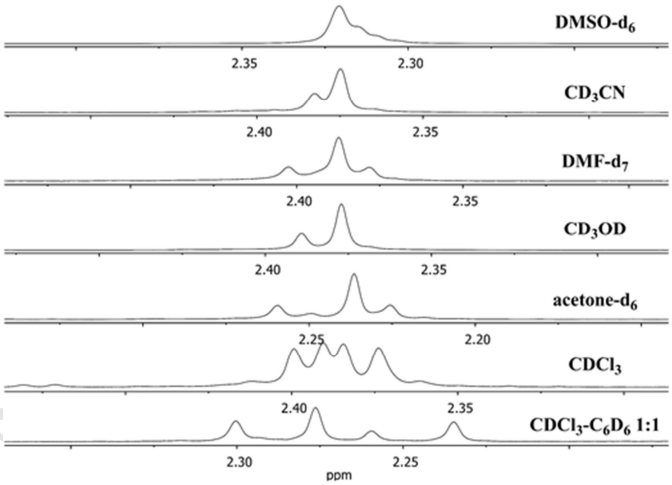

Figure 8. Methyl protons (Region D) of the ^{1}H NMR spectra of **1** in different solvents at 25 ˚C.

Differences in the polarity of the mixtures also affect the *Z/E* isomer populations. The absolute *ZZ:EZ:EE* ratios and their relative energies can be determined from the deconvolution of the methyl signals in the $C_6D_6/CDCl_3$ mixture, in $CDCl_3$ and in acetone–d_6. Table 5 shows that the most stable conformer is solvent-dependent. In $CDCl_3$ all conformers have similar populations (30:39:31) being the *EZ* the preferential one. In $CDCl_3$–C_6D_6 and acetone–d_6, the *ZZ* conformer is the most stable. In these two latter cases, the energy difference between the *ZZ* and *EZ* conformers and between the *EZ* and *EE* ones are similar but not equal, showing that the configuration of one formamide is not independent from the configuration of the other one.

Table 5. *ZZ/EZ/EE* ratio of **1** in different solvents at 25 °C

Solvent	ε	μ	*ZZ:EZ:EE* (%)[a]	$\Delta G_{ZZ}/\Delta G_{EZ}/\Delta G_{EE}$ (kJ/mol)[b]
$CDCl_3$-C_6D_6 1:1 (V/V)	3.50	-	49:32:19	0.0 / 1.1 / 2.4
$CDCl_3$	4.81	1.15	30:39:31	0.7 / 0.0 / 0.6
Acetone–d_6	20.7	2.85	72:21:7	0.0 / 3.1 / 5.7

[a] Determined by ^{1}H NMR deconvolution of methyl signals at 25 °C, without calibration curve.

[b] Related to the most stable conformer, at 25 °C.

In other solvents, the *ZZ:EZ:EE* populations cannot be calculated independently. Anyway, the overall *Z/E* ratio can be obtained from the integrals for the CHO [*E*] and CHO [*Z*] signals (Table 6). In this case, the sides of the molecule may be considered not communicated, and thus each formanilide moiety is interpreted as an independent entity with *E* or *Z* configuration (denoted for simplicity as *E* or *Z* conformer from now on).

Except for $CDCl_3$, in every solvent the *Z* configuration is preferred over the *E* one, with a fixed 75:25 approximate ratio in polar solvents. These results are usually observed for simple formanilides with no 2-substituent, with the *Z* isomer being predominant in DMSO–d_6 [27–31,47,48], acetone–d_6 [36] and CD_3OD [36] and *Z/E* ratios close to 1:1 in $CDCl_3$ [36,47,49,50].

Table 6. Overall Z/E ratio of **1** in different solvents at 25 °C

Solvent	ε	μ	*Z:E* (%)[a]
$CDCl_3$–C_6D_6 1:1 (V/V)	3.50	-	64:36
$CDCl_3$	4.81	1.15	50:50
Acetone–d_6	20.7	2.85	76:24
CD_3OD	32.7	1.70	74:26
DMF–d_7	36.7	3.86	77:23
CD_3CN	37.5	3.45	74:26
DMSO–d_6	46.7	3.90	73:27

[a] Determined by ^{1}H NMR integration of aldehyde signals at 25 °C, without calibration curve.

The spectra of compound **1** were also measured in different mixtures of $CDCl_3$/CD_3OD to evaluate the effect of the solvent polarity on the chemical shift and the number of peaks for each hydrogen. For all signals, the possibility of discrimination of each peak regarding the farthest formamide configuration diminishes as solvent polarity increases. This result is consistent with those obtained in other solvents, showing that the dielectric properties of the solvent seem to be the main shielding factor of anisotropic effects. This behavior can be observed for the methyl protons in Figure 9 and for other regions in Figures S14–S16.

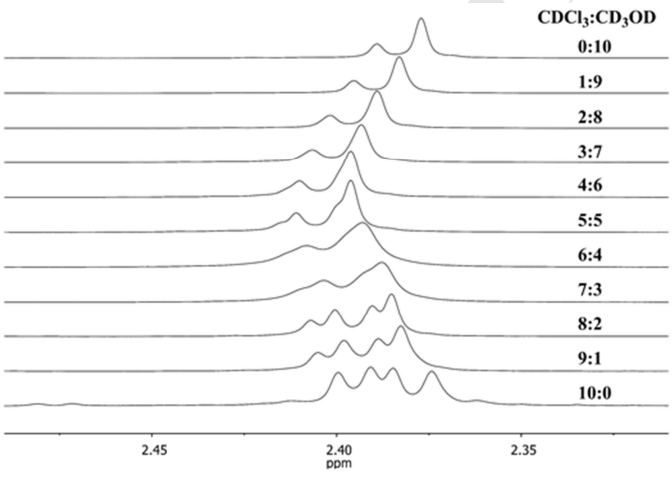

Figure 9. Methyl protons (Region D) of the ^{1}H NMR spectra of **1** in different $CDCl_3$–CD_3OD (V/V) mixtures at 25 °C.

As previously noted, a deconvolution of the four peaks can only be done in the least polar mixtures, but the overall *Z/E* ratio can be measured in all of them (Table 7). The *Z* population increases with the dielectric constant at low polarities, until it reaches an approximately constant value of 75 % from ε ≈ 20, as observed for other solvents.

Table7. Overall Z/E ratio of **1** in $CDCl_3$-CD_3OD mixtures (V/V) at 25 °C

$CDCl_3$:CD_3OD (V/V)	ε	*Z:E* (%)[a]
10:0	4.81	50:50
9:1	7.60	62:38
8:2	10.4	65:35
7:3	13.2	68:32
6:4	16.0	73:27
5:5	18.8	76:24
4:6	21.5	76:24
3:7	24.3	76:24
2:8	27.1	76:24
1:9	29.9	75:25
0:10	32.7	74:26

[a] Determined by ^{1}H NMR integration of aldehyde signals at 25 °C, without calibration curve.

From the data presented in Table 7, the Gibbs free energy of equilibria were estimated ($\Delta G^\circ_{E \leftrightarrows Z} = -RT.\ln K_{E \leftrightarrows Z}$), assuming that both sides of the molecule were independent. The graphical representation of these results for the least polar mixtures (Figure 10) shows a linear relationship with the Kirkwood function (ε–1)/(2ε+1), demonstrating that purely electrostatic solute/solvent interactions are the main factor defining the *Z/E* ratio in the low solvent polarity regime [51–53]. This behavior is not maintained

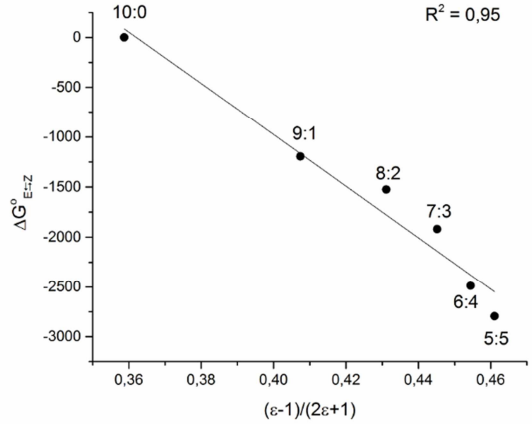

Figure 10. Gibbs free energy of *E/Z* equilibria plotted against the Kirkwood function (ε–1)/(2ε+1) for the least polar $CDCl_3$–CD_3OD mixtures (V/V) at 25 °C.

at high polarity solvents, which shows that other effects must be present.

The increase in the overall *Z/E* ratio in polar solvents was also observed by theoretical calculations. Table 8 shows the calculated ΔG values for each conformer related to the most stable isomer in $CDCl_3$ and DMSO–d_6, and its relative populations given by a Boltzmann analysis. Even when the values do not exactly match, the general trend of the increase of the *Z/E* ratio in DMSO–d_6 with respect to $CDCl_3$ is kept, and the fact that the sides of the molecule are mutually dependent is respected as well.

Table 8. Calculated and experimental free energies of formation (related to the most stable conformer) and population rates for **1** in $CDCl_3$ and DMSO–d_6.

Solvent	ΔG (kJ/mol)	Population at 298K	$(Z/E)_{calc}$	$(Z/E)_{exp}$
	ZZ: 0.00	76.8 %		
$CDCl_3$	*EZ*: 3.55	18.3 %	6.1	1.0
	EE: 6.82	4.9 %		
	ZZ: 0.00	82.0 %		
DMSO-d_6	*EZ*: 4.10	15.7 %	8.9	2.7
	EE: 8.83	2.3 %		

2.4. Variable Temperature NMR spectra

The ^{1}H NMR spectra of **1** in the formamide region in DMSO–d_6, taken in the temperature interval 298–353 K, show peak broadening and a slight change in chemical shifts as temperature rises (Figure 11). The coalescence temperature is not reached, and thus it is necessary to perform a complete line shape analysis (CLSA) of some of the exchanging peaks in the slow–intermediate regime. Peak deconvolution of the CHO signals was achieved using the MestReNova software, allowing the determination of the kinetic constants at each temperature.

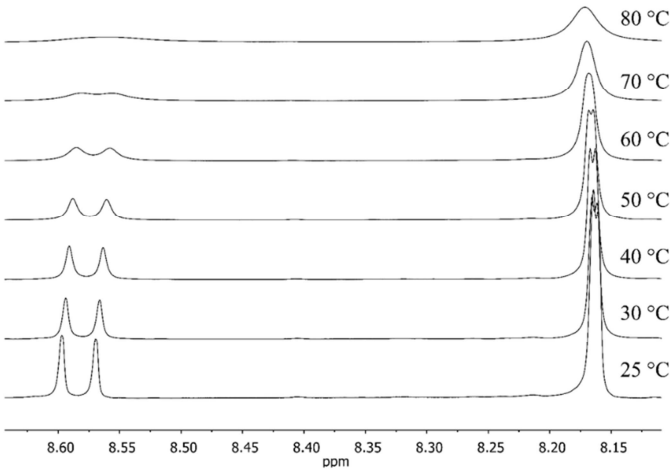

Figure 11. Aldehyde protons of the ^{1}H NMR spectra of **1** in DMSO–d^6 at different temperatures.

For a two-site exchange with unequal populations, the rate constants k_i (*i*: *E*, *Z* for *E*→*Z* and *Z*→*E* respectively) can be estimated considering the difference between the observed peak widths $\Delta\nu_{½}$ at each temperature T and the natural bandwidth in the slow exchange limit at 25º C (T°), which is assumed to account for all transverse relaxation mechanisms other than chemical exchange (Eq. 1) [54].

$$\Delta\upsilon_{½}^{exp\,(T),i} = \Delta\upsilon_{½}^{obs(T),i} - \Delta\upsilon_{½}^{obs(T°),i} = \frac{k_i}{\pi} \qquad (1)$$

In this case, the ratio between the constants k_E and k_Z should be given by the equilibrium constant $K_{E\leftrightarrows Z}$, which can be determined by the population of each configuration p_i and thus the integration of peaks (Eq. 2).

$$\frac{k_E}{k_Z} = \frac{p_Z}{p_E} = K_{E\leftrightarrows Z} \qquad (2)$$

The results for the estimated rate and equilibrium constants of **1** in DMSO–d_6 at different temperatures are given in Table 9. Kinetic constants are in the order of 1–100 s^{-1} (lifetimes of 10 ms – 1 s), and estimation of the equilibrium constants from rate constants results in no more than a 30% error with respect to the values obtained by integration.

From CLSA data it is possible to estimate the activation energy parameters for the forward and reverse reactions using the Eyring equation (Eq. 3), assuming κ = 1. Plotting ln (*k*/T) against 1000/T (Figure 12) allows the determination of enthalpy and entropy of activation, $\Delta H^{\neq}$ and $\Delta S^{\neq}$, which are obtained from the slope and intercept of the linear regression, respectively.

$$k = \kappa\frac{k_B T}{h} e^{-\Delta G^{\neq}/RT} \qquad (3)$$

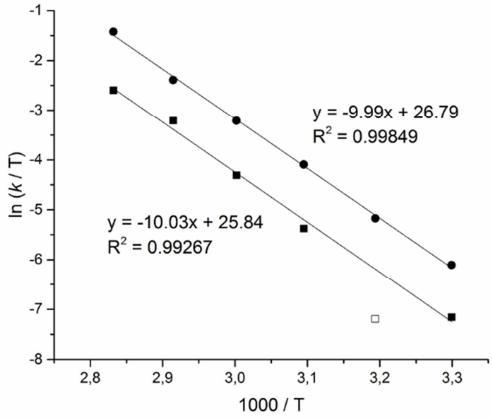

Figure 12. Eyring plot for **1** in DMSO-d^6 solution for E→Z (●) and Z→E (■) rotations. One data point (□) was omitted in the calculations (see Supporting Information).

The results for the activation parameters are shown in Table 10. Enthalpies of activation are very similar for both processes, indicating that ΔH is approximately zero in DMSO–d_6. This is consistent with the fact that the ratio from major to minor isomer in DMSO-d_6, obtained by peak integration, does not change upon temperature increase, and demonstrates that conformer equilibrium is an entropically driven process. At room temperature, $K_{E\leftrightarrows Z}$ = 2.7, and thus ΔS is estimated as 8.3 $J.K^{-1}mol^{-1}$, in close agreement with the value obtained from CLAS of 7.9 $J.K^{-1}mol^{-1}$.

Table 10. Activation parameters of **1** in DMSO–d_6 obtained from Eyring's plot.

	$\Delta H^{\neq}$ / kJ.mol^{-1}	$\Delta S^{\neq}$ / J.K^{-1}mol^{-1}
E→Z	83.0	25.1
Z→E	83.3	17.2

Estimated values for $\Delta G^{\neq}$ at 298 K in DMSO–d_6 are 75.5 and 78.2 kJ.mol^{-1} for *E*→*Z* and *Z*→*E*, respectively, which lie in the usual interval of 63–96 kJ.mol^{-1} for Gibbs free energies of activation for hindered amide rotation [55]. ΔG° for the *E*⇆*Z* equilibrium is estimated thus as –2.7 kJ.mol^{-1}, result with less than 10% error with respect to that calculated from integration (–2.5 kJ.mol^{-1}).

3. Conclusions

The current work provides full description of the complex array of signals in the NMR spectra of a TB diformamide **1** and offers novel evidence about the dependence of the moieties on each side of this type of scaffold. This behavior is originated by

the presence of three conformers in equilibrium, which correspond to the possible configurations of the amide moiety, and is consistent with long–range anisotropic effects generated by the carbonyl groups. DFT calculations allowed the complete assignment of NMR spectra and confirmed the experimental capability of signal distinction. In addition, our work reports the study of solvent polarity and temperature effects on the signals. The detailed conformational analysis shows that the *E/Z* ratio is mainly determined by electrostatic interactions in the low polarity regime and that it adopts a constant value in polar solvents. Activation parameters determined in DMSO demonstrate that in this case conformer equilibrium is an entropically driven process.

To the best of our knowledge, this is the first systematic conformational analysis of this kind of model system and paves the way for future promising studies through the design of new TB derivatives with amide bonds.

Acknowledgments

This work was supported by Agencia Nacional de Promoción Científica y Tecnológica (PICT 2013-2331 to J.A.R.) and Universidad de Buenos Aires (UBACyT 20020130100826BA to J.A.R.).

References and notes

[1] S. Sergeyev. Recent Developments in Synthetic Chemistry, Chiral Separations, and Applications of Tröger's Base Analogues, Helv. Chim. Acta 92 (2009) 415–444.

[2] Ö. V. Rúnarsson, J. Artacho, K. Wärnmark. The 125th Anniversary of the Tröger's Base Molecule: Synthesis and Applications of Tröger's Base Analogues, European J. Org. Chem. (2012) 7015–7041.

[3] B. Dolensky, J. Elguero, V. Král, C. Pardo, M. Valík. Current Tröger's Base Chemistry, Adv. Heterocycl. Chem. 93 (2007) 1–56.

[4] S. Sergeyev, D. Didier, V. Boitsov, A. Teshome, I. Asselberghs, K. Clavs, C. M. L. Vande Velde, A. Plaquet, B. Champagne. Symmetrical and Nonsymmetrical Chromophores with Tröger's Base Skeleton: Chiroptical, Linear, and Quadratic Nonlinear Optical Properties— A Joint Theoretical and Experimental Study, Chem. - A Eur. J. 16 (2010) 8181–8190.

[5] I. Neogi, S. Jhulki, A. Ghosh, T. J. Chow, J. N. Moorthy. Bifunctional organic materials for OLEDs based on Tröger's base: Subtle structural changes and significant differences in electroluminescence, Org. Electron. physics, Mater. Appl. 15 (2014) 3766–3772.

[6] Z. Wu, M. Tang, T. Tian, J. Wu, Y. Deng, X. Dong, Z. Tan, X. Weng, Z. Liu, C. Wang, X. Zhou. A specific probe for two-photon fluorescence lysosomal imaging, Talanta 87 (2011) 216–221.

[7] B. Reddy Manda, M. Alla, R. J. Ganji, A. Addlagatta. Discovery of Tröger's base analogues as selective inhibitors against human breast cancer cell line: Design, synthesis and cytotoxic evaluation, Eur. J. Med. Chem. 86 (2014) 39–47.

[8] C. Benkhäuser, A. Lützen. Self-assembly of heteroleptic dinuclear metallosupra- molecular kites from multivalent ligands via social self-sorting, Beilstein J. Org. Chem 11 (2015) 693–700.

[9] S. Shanmugaraju, C. Dabadie, K. Byrne, A. J. Savyasachi, D. Umadevi, W. Schmitt, J. A. Kitchen, T. Gunnlaugsson, Z.-M. Su. A supramolecular Tröger's base derived coordination zinc polymer for fluorescent sensing of phenolic-nitroaromatic explosives in water, Chem. Sci. 8 (2017) 1535–1546.

[10] S. Banerjee, S. A. Bright, J. A. Smith, J. Burgeat, M. Martinez-Calvo, D. C. Williams, J. M. Kelly, T. Gunnlaugsson. Supramolecular Approach to Enantioselective DNA Recognition Using Enantiomerically Resolved Cationic 4□Amino-1,8-naphthalimide-Based Tröger's Bases, J. Org. Chem. 79 (2014) 9272–9283.

[11] E. M. Boyle, S. Comby, J. K. Molloy. Thiourea Derived Tröger's Bases as Molecular Cleft Receptors and Colorimetric Sensors for Anions, J. Org. Chem. 78 (2013) 8312–8319.

[12] F. Vögtle. *Fascinating Molecules in Organic Chemistry*, Wiley, Chichester, 1992.

[13] C. Pardo, I. Alkorta, J. Elguero. A DFT study of the geometric, magnetic NMR chemical shifts and optical rotation properties of Tröger's bases, Tetrahedron Asymmetry 17 (2006) 191–198.

[14] R. Yuan, M. qi Li, J. biao Xu, S. ying Huang, S. liang Zhou, P. Zhang, J. juan Liu, H. Wu. Synthesis and optical properties of novel Tröger's base derivatives, Tetrahedron 72 (2016) 4081–4084.

[15] B. Bhayana, M. R. Ams. Effect of Diazocine Bridgehead Modification on the Folding of the Wilcox Molecular Torsion Balance: A View from a Different Angle, J. Org. Chem. 76 (2011) 3594–3596.

[16] F. R. Fischer, P. a Wood, F. H. Allen, F. Diederich. Orthogonal dipolar interactions between amide carbonyl groups, Proc. Natl. Acad. Sci. U. S. A. 105 (2008) 17290–17294.

[17] B. G. Janesko, M. R. Ams. Dispersion-corrected DFT study of methano and ethano bridged Wilcox torsion balances, Theor. Chem. Acc. 133 (2014) 1–11.

[18] C. L. Ramírez, C. Pegoraro, L. Trupp, A. Bruttomesso, V. Amorebieta, D. M. A. Vera, A. R. Parise. Charge transfer properties of Tröger base derivatives, Phys. Chem. Chem. Phys. 13 (2011) 20076–20080.

[19] L. N. Monsalve, A. V. Medrano, F. Golmar, L. Trupp, A. R. Parise, A. Bruttomesso. Performance of Solution Processed Tröger Base Bis(triarylamine) Derivative as Channel for Field Effect Transistors, Smart Syst. Integr. 2016 - Int. Conf. Exhib. Integr. Issues Miniaturized Syst. SSI 2016 (2016) .

[20] R. J. Abraham, L. Griffiths, M. Perez. 1H NMR spectra. Part 30: 1H chemical shifts in amides and the magnetic anisotropy, electric field and steric effects of the amide group, Magn. Reson. Chem. 51 (2013) 143–155.

[21] U. Kiehne, T. Weilandt, A. Lutzen. Diastereoselective Self-Assembly of Double-Stranded Helicates from Tröger's Base Derivatives, Org. Lett. 9 (2007) 1283–1286.

[22] D. G. Rivera, L. A. Wessjohann. Supramolecular Compounds from Multiple Ugi Multicomponent Macrocyclizations: Peptoid-based Cryptands, Cages, and Cryptophanes, J. Am. Chem. Soc. 128 (2006) 7122–7123.

[23] L. Chabaud, J. Clayden, M. Helliwell, A. Page, J. Raftery, L. Vallverdú. Conformational studies of tertiary oligo-m-benzanilides and oligo-p-benzanilides in solution, Tetrahedron 66 (2010) 6936–6957.

[24] I. Okamoto, M. Terashima, H. Masu, M. Nabeta, K. Ono, N. Morita, K. Katagiri, I. Azumaya, O. Tamura. Acid-induced conformational alteration of cis-preferential aromatic amides bearing N-methyl-N-(2-pyridyl) moiety, Tetrahedron 67 (2011) 8536–8543.

[25] I. Okamoto, M. Nabeta, T. Minami, A. Nakashima, N. Morita, T. Takeya, H. Masu, I. Azumaya, O. Tamura. Acid-induced conformational switching of aromatic N-methyl-N-(2-pyridyl)amides, Tetrahedron Lett. 48 (2007) 573–577.

[26] M. Tafazzoli, A. Ziyaei-Halimjani, M. Ghiasi, M. Fattahi, M. R. Saidi. Dynamic NMR studies of N-benzoyl pyrrolidine and N-benzoyl piperidine derivatives, J. Mol. Struct. 886 (2008) 24–31.

[27] C. Zhang, Z. Xu, T. Shen, G. Wu, L. Zhang, N. Jiao. Mn-promoted Aerobic Oxidative C-C Bond Cleavage of Aldehydes with Dioxygen Activation: A Simple Synthetic Approach to Formamide, Org. Lett. 14 (2012) 2362–2365.

[28] J. Liang, F. Hu, X. Lv, Z. Chen, Z. Chen, J. Yin, G. A. Yu, S. H. Liu. Synthesis, characterization and mechanochromic behavior of binuclear gold (I) complexes with various diisocyano bridges, Dye. Pigment. 95 (2012) 485–490.

[29] D. Michalik, A. Schaks, L. A. Wessjohann. One-Step Synthesis of Natural Product-Inspired Biaryl Ether-Cyclopeptoid Macrocycles by Double Ugi Multiple-Component Reactions of Bifunctional Building Blocks, European J. Org. Chem. (2007) 149–157.

[30] J. Hyvl, J. Srogl. Copper-Catalyzed Activation of Disulfides as a Key Step in the Synthesis of Benzothiazole Moieties, European J. Org. Chem. (2010) 2849–2851.

[31] D. W. Price, S. M. Dirk, F. Maya, J. M. Tour. Improved and new syntheses of potential molecular electronics devices, Tetrahedron 59 (2003) 2497–2518.

[32] I. Azumaya, K. Yamaguchi, I. Okamoto, H. Kagechika, K. Shudo. Total Asymmetric Transformation of an N-Methylbenzamide, J. Am. Chem. Soc. 117 (1995) 9083–9084.

[33] R. Quintanilla-Licea, J. F. Colunga-Valladares, A. Caballero-Quintero, C. Rodríguez-Padilla, R. Tamez-Guerra, R. Gómez-Flores, N. Waksman. NMR Detection of Isomers Arising from Restricted Rotation of the C-N Amide Bond of N-Formyl-o-toluidine and N,N'-bis- Formyl-o-tolidine, Molecules 7 (2002) 662–673.

[34] L. A. Konup, I. P. Konup, V. E. Sklyar, K.N. Kosenko, V. P. Gorodnyuk, G. V. Fedorova, E. I. Nazarov, S. A. Kotlyar. Antimicrobial activity of aliphatic and aromatic crown ethers, Pharm. Chem. J. 23 (1989) 402–408.

[35] L. Yang, K. Cheung, A. Mayr. Synthesis of several functionalized cis-diisocyanide and fac-triisocyanide metal complexes, J. Organomet. Chem. 585 (1999) 26–34.

[36] V. Pace, K. De La Vega-Hernández, E. Urban, T. Langer, K. De La Vega-Hernández, E. Urban, T. Langer. Chemoselective Schwartz Reagent Mediated Reduction of Isocyanates to Formamides, Org. Lett. 18 (2016) 2750–2753.

[37] D. W. Agnew, M. Gembicky, C. E. Moore, A. L. Rheingold, J. S. Figueroa. Robust, Transformable, and Crystalline Single-Node Organometallic Networks Constructed from Ditopic m-Terphenyl Isocyanides, J. Am. Chem. Soc. 138 (2016) 15138–15141.

[38] K. M. El-Shaieb, A. F. E. Mourad, A. A. Hassan. 4,15-Diamino[2.2]paracyclophane as a useful precursor for the synthesis of novel pseudogeminal [2.2]paracyclophane compounds, Zeitschrift fur Naturforsch. - Sect. B J. Chem. Sci. 70 (2015) 843–850.

[39] Z. Chen, J. Zhang, M. Song, J. Yin, G.-A. Yu, S. H. Liu. A novel fluorene-based aggregation-induced emission (AIE)-active gold(I) complex with crystallization-induced emission enhancement (CIEE) and reversible mechanochromism characteristics, Chem. Commun. 51 (2015) 326–329.

[40] W. Kohn, L. J. Sham. Self-Consistent Equations Including Exchange and Correlation Effects, Phys. Rev. 140 (1965) A1133–A1138.

[41] A. D. Becke. Density-functional thermochemistry.III. The role of exact exchange, J. Chem. Phys. 98 (1993) 5648.

[42] C. Lee, W. Yang, R. G. Parr. Development of the Colle-Salvetti correlation-energy formula into a functional of the electron density, Phys. Rev. B 37 (1988) 785–789.

[43] R. G. Parr, W. Yang. Oxford University Press, New York 1989, p 352.

[44] B. Mennucci, J. Tomasi. Continuum solvation models: A new approach to the problem of solute s charge distribution and cavity boundaries, J. Chem. Phys. 106 (1997) 5151–5158.

[45] E. Cances, B. Mennucci, J. Tomasi. A new integral equation formalism for the polarizable continuum model: Theoretical background and applications to isotropic and anisotropic dielectrics, J. Chem. Phys. 107 (1997) 3032.

[46] M. Cossi, V. Barone, B. Mennucci, J. Tomasi. Ab initio study of ionic solutions by a polarizable continuum dielectric model, Chem. Phys. Lett. 286 (1998) 253–260.

[47] T. B. Nguyen, J. Sorres, M. Q. Tran, L. Ermolenko, A. Al-Mourabit. Boric Acid – A Highly Efficient Catalyst for Transamidation of Carboxamides with Amines, Org. Lett. 14 (2012) 3202–3205.

[48] S. Batuta, N. A. Begum. Solvent and catalyst free N-formylations of amines at ambient condition: Exploring the usability of aromatic formates as N-formylating agents, Synth. Commun. 47 (2017) 137–147.

[49] Y. Nishikawa, H. Nakamura, N. Ukai, W. Adachi, O. Hara. Tetraethylorthosilicate as a mild dehydrating reagent for the synthesis of N-formamides with formic acid, Tetrahedron Lett. 58 (2017) 860–863.

[50] C. Voss, C. Scholz, S. Knorr, P. Beck, M. L. Stein, A. Zall, U. Kuckelkorn, P. M. Kloetzel, M. Groll, K. Hamacher, B. Schmidt. α-Keto Phenylamides as P1'-Extended Proteasome Inhibitors, ChemMedChem (2014) 2557–2564.

[51] D. S. Choi, Y. S. Chong, D. Whitehead, K. D. Shimizu. Molecules with Shape Memory Based on Restricted Rotation, Org. Lett. 3 (2001) 3757–3760.

[52] J. Leis, K. D. Klika, M. Karelson. Solvent Polarity Effects on the E/Z Conformational Equilibrium of N-1-naphthylamides, Tetrahedron 54 (1998) 7497–7504.

[53] C. Reichardt, T. Welton. Solvents and Solvent Effects in Organic Chemistry, 4th ed., Wiley, Weinheim, 2011.

[54] T. D. W. Claridge. High-Resolution NMR Techniques in Organic Chemistry, 3rd ed., Elsevier, Oxford, 2016.

[55] J. Á. Bisceglia, M. Cruz Mollo, L. R. Orelli. E/Z equilibrium in tertiary amides. Part 2: N-acyl-N0-arylhexahydropyrimidines, J. Mol. Struct. 966 (2010) 79–84.

Table 9. Rate and equilibrium constants of 1 in DMSO-d_6 estimated by CLSA at different temperatures.

T / K	$k_{E\rightarrow Z}$ / s^{-1}	$k_{Z\rightarrow E}$ / s^{-1}	$K_{E\rightleftarrows Z}$ [a]	$K_{E\rightleftarrows Z}$ [b]
303.1	0.68	0.24	2.9	2.7
313.1	1.77	[c]	[c]	2.7
323.1	5.39	1.49	3.6	2.7
333.1	13.4	4.48	3.0	2.7
343.1	31.5	13.7	2.3	2.7
353.1	85.2	26.3	3.2	2.7

[a] Determined as the ratio between the constants $k_{E\rightarrow Z}$ and $k_{Z\rightarrow E}$.

[b] Determined by ^{1}H NMR integration of aldehyde signals at 25 °C, without calibration curve.

[c] Omitted in the calculations (see Supporting Information).

1- We present the synthesis and full NMR analysis of a diformamide TB derivative **1**.
2- **1** displays a complex array of signals originated by the presence of three conformers.
3- DFT calculations and 2D NMR experiments allowed the full assignment of ^{1}H NMR.
4- Solvent polarity and temperature effects were analyzed.
5- **1** serves as a probe for long–range anisotropic effects generated by carbonyl groups.